PROCEEDINGS of the
23rd International Congress on Acoustics

9 to 13 September 2019 in Aachen, Germany

Theoretical and experimental analysis of a skyhook damper for active control of sound transmission

Neven ALUJEVIĆ[1]; Steven CLAES[2]; Martina ŠIMAG[1]; Paul SAS[2]

[1] University of Zagreb, Croatia

[2] KU Leuven, Belgium

ABSTRACT

In this paper active control of sound transmission through a double panel is considered. The active control system consists of one accelerometer mounted on the radiating panel whose time-integrated and amplified output is used as the error signal to drive a voice-coil actuator that reacts between the source and the radiating panel. Effects of one such active damper in the centre of the double panel system are considered, although, in principle, it could be repeated in the *x*-*y* plane and then used in the centralised, distributed or a decentralised manner. Theoretical and an experimental results are presented and compared. In the theoretical part, the mobility matrix model is used to investigate the stability of the feedback loop and to calculate the sound transmission ratio with and without control. It is shown that large reductions of the sound transmission ratio are possible, however only if the natural frequency of the fundamental source panel mode is higher than the natural frequency of the fundamental radiating panel mode. The experimental part of the study is carried out on the prototype active panel system and the measured result fully corroborate theoretical predictions.

Keywords: Sound, Vibration, Active control of sound transmission

1. INTRODUCTION

The construction of transportation vehicles such as cars, aircraft or helicopters typically involves a considerable number of thin-walled and lightweight structural elements. From a vibroacoustic point of view, such structural elements are efficient sound radiators and transmitters, particularly in the low frequency range (1). There are several reasons why the low-frequency sound radiation and transmission pose a particularly challenging problem in lightweight, thin-walled structures. First, the sound transmission through panels and similar structures is characterised by the so-called mass law. The mass law imposes a decrease of the sound transmission ratio with the increase in frequency (2). At low frequencies, however, the sound transmission ratio remains relatively high. In fact, the sound transmission ratio through panel-like structures at low frequencies is largely controlled by structural resonances so that both vibrations and sound transmission are high. The radiation of sound is particularly high due to the lightly damped odd-odd structural modes characterised by high volume velocity (3). Second, the mass law also imposes a decrease of the sound transmission ratio with the increase of mass per unit area of the partition (2), imposing fundamental physical limitations to controlling the transmission of sound using lightweight structures. The combination of the two effects two therefore causes problems in terms of high structural vibrations and the consequent high sound transmission ratio of thin-walled lightweight structures at low frequencies.

These vibration and noise problems are traditionally solved by passive means (4). For example, the resonance effect can be reduced by increasing structural damping using dissipative treatments. These treatments are typically consisted of constrained damping layers of viscoelastic materials that are glued to the structure. The problem with this technique is that it is typically targets only higher-order modes of the structure and significantly increases the weight and cost of the product. Alternatively, thin-walled structures can be equipped with single or multiple layers of sound absorbing

[1] neven.alujevic@fsb.hr

materials (4). These materials are typically open cell rubber foams or melamine sponges which absorb noise by friction within the cell structure. Porous open cell foams are highly effective noise absorbers across a broad range of medium to high frequencies (5). At low frequencies their performance deteriorates. This is because of long acoustic waves at low frequencies. When the acoustic wavelength becomes much larger than the thickness of the sound absorbing layer, the waves efficiently penetrate through the layer. In conclusion, the control of sound transmission through lightweight, thin-walled structures at low frequencies requires a special attention.

In this paper active control of sound transmission is considered through a double panel. A direct velocity feedback control scheme with non-collocated sensor-actuator arrangement is used. It is shown that active damping can be generated which reduces the sound transmission due to low-order structural modes. In Section 2 the mathematical model for the theoretical analysis is formulated whereas in Section 3 the setup for the experimental measurement campaign is described. The results of the theoretical and experimental analyses are contrasted and discussed in Section 4.

2. MATHEMATICAL MODEL

The mathematical model is based on the mobility-impedance approach (4,6). To this end, it is assumed that the system can be divided into three components: the source panel, the radiating panel and the acoustical transmission path. The acoustical path is due to the sound transmission through the air confined between the radiating and the source panel. Each of these components is modelled using point and transfer mobility or impedance functions. The acoustical transmission path is modelled using transfer impedances between a finite number of cavity elements that are adjacent to the surfaces of the panels. The excitation of the source panel by the incident acoustic wave and the radiated sound power from the radiating panel are also calculated by assuming that the two panels are divided into the same number of elements. This number is obtained by choosing element dimensions to be $l_{x,e}=l_x/(4M)$ and $l_{y,e}=l_y/(4N)$ where M and N are the highest modal orders used in calculations. The mobility model scheme is given in Figure 1.

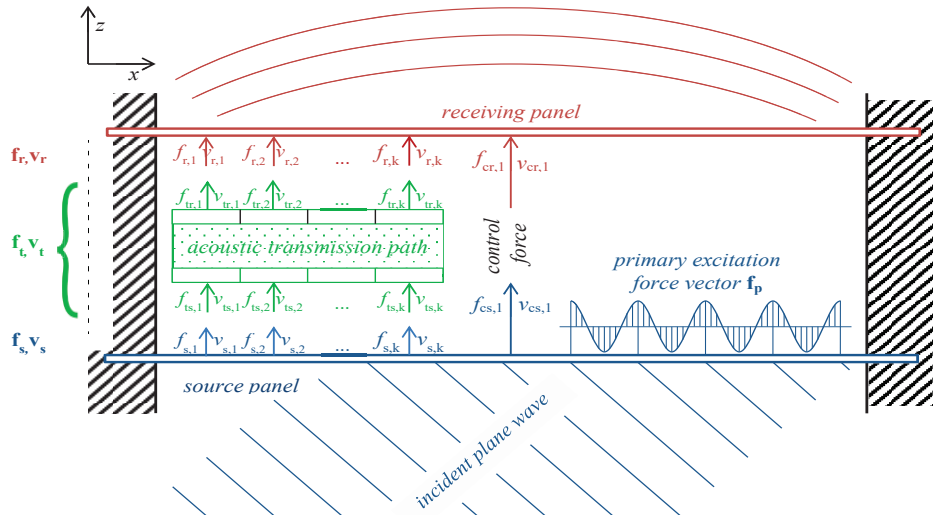

Figure 1 – The mobility model scheme

The model considers only out of plane displacements/velocities and forces at the various types of junctions and at the centres of the plates and cavity elements. The time harmonic displacement or force are given by $w(t)=\mathrm{Re}\{w(\omega)e^{j\omega t}\}$ or $f(t)=\mathrm{Re}\{f(\omega)e^{j\omega t}\}$, where ω is the circular frequency in [rad/s] and $j=-1^{1/2}$. Thus $w(t)$ and $f(t)$ are the time-harmonic displacement and force functions while $w(\omega)$ and $f(\omega)$ are the complex frequency-dependent displacement and force phasors. In order to simplify the mobility formulation used in this study, the time harmonic dependence is implicitly assumed in the mathematical expressions which are therefore formulated in terms of the frequency-dependent phasors. Also, the first derivative of the time-harmonic functions, for example the linear out of plane velocity, $\dot{w}(t)=\mathrm{Re}\{j\omega w(\omega)e^{j\omega t}\}$ is represented by velocity frequency dependent phasors $\dot{w}(\omega)=j\omega w(\omega)$. The velocity and force phasors at the centres of the elements are grouped in the following two column vectors:

$$\mathbf{v} \equiv \left\{\dot{w}_1, \dot{w}_2, \ldots \dot{w}_j, \ldots \dot{w}_{k-1}, \dot{w}_k\right\}^T, \qquad \mathbf{f} \equiv \left\{N_{z1}, N_{z2}, \ldots N_{zj}, N_{zk-1}, N_{zk}\right\}^T \tag{1}$$

where $\dot{w}_j$ is the complex amplitude of the linear velocity along the z axis, and N_{zj} is the complex amplitude of the force in the z direction, at the j-th element. The two panels are also excited by means of p control forces. The velocity and control force phasors at the control positions in the source and radiating panels are grouped in the following two column vectors:

$$\mathbf{v}_c \equiv \left\{\dot{w}_1, \dot{w}_2, ...\dot{w}_j, ...\dot{w}_{p-1}, \dot{w}_p\right\}^T, \qquad \mathbf{f}_c \equiv \left\{N_{z1}, N_{z2}, ...N_{zj}, N_{zp-1}, N_{zp}\right\}^T \tag{2}$$

It is thus in principle possible to model a number of control forces acting on the source and/or on the radiating panel. In the remaining of the paper, however, a single reactive control force, located at the x,y centre of the double panel is considered. The surface boundaries that the air cavity shares with the source and the radiating plate are modelled using a finite number k of small elements, such that the element dimensions are considerably smaller than the shortest acoustic wavelength in the cavity. The lateral surfaces of the air cavity are assumed to be rigid walls. Each of the top and bottom surface elements can only vibrate in the direction normal to the surfaces themselves and their velocities and forces are defined at the geometrical centres of the elements. These junction vectors are grouped together to form four combined vector pairs. These four groups are: the source velocity vector $\mathbf{v}_s$ and the source force vector $\mathbf{f}_s$, the radiating velocity vector $\mathbf{v}_r$ and the radiating force vector $\mathbf{f}_s$; the transmission system velocity vector $\mathbf{v}_t$ and the transmission system force vector $\mathbf{f}_t$; and finally, the control velocity vector $\mathbf{v}_c$ and the control force vector $\mathbf{f}_c$. The four groups of vectors are given by:

$$\mathbf{v}_s \equiv \left\{v_{s,1} \quad v_{s,2} \quad \cdots \quad v_{s,k}\right\}^T, \qquad \mathbf{f}_s \equiv \left\{f_{s,1} \quad f_{s,2} \quad \cdots \quad f_{s,k}\right\}^T \tag{3}$$

$$\mathbf{v}_r \equiv \left\{v_{r,1} \quad v_{r,2} \quad \cdots \quad v_{r,k}\right\}^T, \qquad \mathbf{f}_r \equiv \left\{f_{r,1} \quad f_{r,2} \quad \cdots \quad f_{r,k}\right\}^T \tag{4}$$

$$\mathbf{v}_t \equiv \left\{\mathbf{v}_{ts} \quad \mathbf{v}_{tr}\right\} \equiv \left\{v_{ts,1} \quad v_{ts,2} \quad \cdots \quad v_{ts,k} \quad v_{tr,1} \quad v_{tr,2} \quad \cdots \quad v_{tr,k}\right\}^T \tag{5}$$

$$\mathbf{f}_t \equiv \left\{\mathbf{f}_{ts} \quad \mathbf{f}_{tr}\right\} \equiv \left\{f_{ts,1} \quad f_{ts,2} \quad \cdots \quad f_{ts,k} \quad f_{tr,1} \quad f_{tr,2} \quad \cdots \quad f_{tr,k}\right\}^T \tag{6}$$

$$\mathbf{v}_c \equiv \left\{\mathbf{v}_{cs} \quad \mathbf{v}_{cr}\right\} \equiv \left\{v_{cs,1} \quad v_{cs,2} \quad \cdots \quad v_{cs,p} \quad v_{cr,1} \quad v_{cr,2} \quad \cdots \quad v_{cr,p}\right\}^T \tag{7}$$

$$\mathbf{f}_c \equiv \left\{\mathbf{f}_{cs} \quad \mathbf{f}_{cr}\right\} \equiv \left\{f_{cs,1} \quad f_{cs,2} \quad \cdots \quad f_{cs,p} \quad f_{cr,1} \quad f_{cr,2} \quad \cdots \quad f_{cr,p}\right\}^T \tag{8}$$

where $v_{s,j}$ and $f_{s,j}$ represent the complex velocities and forces for the j-th source panel element, $v_{r,j}$ and $f_{r,j}$ represent the complex velocities and forces at the j-th radiating panel element, $v_{ts,j}$ and $f_{ts,j}$ represent the complex velocities and forces for the j-th acoustic element on the source panel junction, $v_{tr,j}$ and $f_{tr,j}$ represent the complex velocities and forces for the j-th acoustic element on the radiating panel junction, $v_{cs,j}$ and $f_{cs,j}$, and finally $v_{cr,j}$ and $f_{cr,j}$ represent the control system complex velocities and forces for the j-th control force at the j-th control point either on the source or on the radiating panel footprint of the control force actuators.

The dynamics of the bare source and radiating panels are modelled using a mobility matrix formulation, so that velocity and force vectors can be expressed in the form:

$$\mathbf{v}_s = \mathbf{Y}_{ss}\mathbf{f}_s + \mathbf{Y}_{sp}\mathbf{f}_p + \mathbf{Y}_{sc}\mathbf{f}_c, \qquad \mathbf{v}_r = \mathbf{Y}_{rr}\mathbf{f}_r + \mathbf{Y}_{rf}\mathbf{f}_f + \mathbf{Y}_{rc}\mathbf{f}_c \tag{9}$$

where $\mathbf{Y}_{ss}$, $\mathbf{Y}_{sp}$, $\mathbf{Y}_{sc}$ and $\mathbf{Y}_{rr}$, $\mathbf{Y}_{rf}$, $\mathbf{Y}_{rc}$ are mobility matrices of the source and the radiating panel, and $\mathbf{f}_p$, $\mathbf{f}_c$, and $\mathbf{f}_f$ are the primary excitation vector, the control force vector, and the flanking excitation vector, respectively. The details on how the mobility matrices used in Eqs. (9) are populated, and also on how the the mobility and impedance matrices introduced in the forthcoming part of the formulation are populated, are given in (6). Furthermore, details on how to calculate the resonance frequencies $\omega_{m,n}$ and mode shapes $\phi_{m,n}$ for rectangular panels having various boundary conditions can be found in (4). The primary and flanking excitation vector are given by:

$$\mathbf{f}_p \equiv \left\{f_{p,1} \quad f_{p,2} \quad \cdots \quad f_{p,k}\right\}^T, \qquad \mathbf{f}_f \equiv \left\{f_{f,1} \quad f_{f,2} \quad \cdots \quad f_{f,k}\right\}^T \tag{10}$$

The flanking excitation vector acting on the radiating panel could be caused by a subsystem connected to it or by an additional flanking path connecting the source panel to the radiating panel. The flanking excitation has not been considered throughout this study covered, so that the flanking excitation vector $\mathbf{f}_f$ is assumed to be a zero vector. If the source plate is excited by a plane acoustic wave, then the components of the primary excitation vector are determined by pressure field generated

by the plane wave over the surface of the source panel:

$$f_{p,j}(x_j, y_j, \omega) = \frac{l_x l_y}{k} P e^{-j\left(k_x x_j + k_y y_j\right)} \tag{11}$$

where P is the amplitude of the plane wave which has an acoustic wave number in the x direction given by $k_x=k\ \sin(\theta)\cos(\phi)$ and in the y direction given by $k_y=k\ \sin(\theta)\sin(\phi)$, where k is the wave number, θ and ϕ are azimuthal and elevation angles, whereas x_j and y_j are coordinates of the geometrical centre of the corresponding element of the source panel. The term $Pe^{-j\left(k_x x_j + k_y y_j\right)}$ in Eq. (11) is the pressure at the geometrical centre of an element while the term $l_x l_y/k$ is the area of the element. Therefore the excitation is modelled by assuming that the pressure field over the surface of the element can be approximated by the pressure at the centre of the element. The dynamics of the transmission system is expressed using the following impedance matrix expression:

$$\mathbf{f}_t = \mathbf{Z}_t \mathbf{v}_t \tag{12}$$

where $\mathbf{Z}_t$ is an impedance matrix of the transmission system. The elements in the $\mathbf{Z}_t$ matrix, due to the nature of the acoustical coupling, are fully populated. Thus the velocity at one element will generate a force, which is caused by pressure fluctuations at the centres of all the other elements, on both source and radiating plates. The source and radiating panel mobility matrices, Eqs.(9), can be grouped together in one equation:

$$\mathbf{v}_{sr} = \mathbf{Y}_{sr,sr}\mathbf{f}_{sr} + \mathbf{Y}_{sr,pf}\mathbf{f}_{pf} + \mathbf{Y}_{sr,c}\mathbf{f}_c \tag{13}$$

where the mobility matrices and the excitation vectors have the form:

$$\mathbf{Y}_{sr,sr} \equiv \begin{bmatrix} \mathbf{Y}_{s,sr} & \mathbf{0} \\ \mathbf{0} & \mathbf{Y}_{r,sr} \end{bmatrix}, \quad \mathbf{Y}_{sr,pf} \equiv \begin{bmatrix} \mathbf{Y}_{s,pf} & \mathbf{0} \\ \mathbf{0} & \mathbf{Y}_{r,pf} \end{bmatrix}, \quad \mathbf{Y}_{sr,c} \equiv \begin{bmatrix} \mathbf{Y}_{s,c} \\ \mathbf{Y}_{r,c} \end{bmatrix}, \quad \mathbf{f}_{pf} \equiv \begin{Bmatrix} \mathbf{f}_p & \mathbf{f}_f \end{Bmatrix}^T \equiv \begin{Bmatrix} \mathbf{f}_p & \mathbf{0} \end{Bmatrix}^T \tag{14}$$

and the velocity and force vectors are given by:

$$\mathbf{v}_{sr} \equiv \begin{Bmatrix} \mathbf{v}_s & \mathbf{v}_r \end{Bmatrix}^T, \quad \mathbf{f}_{sr} \equiv \begin{Bmatrix} \mathbf{f}_s & \mathbf{f}_r \end{Bmatrix}^T \tag{15}$$

where $\mathbf{v}_{sr}$ and $\mathbf{f}_{sr}$ are respectively the source-radiating velocity vector and the source-radiating force vector. The source-radiating vectors are related to the corresponding coupling system vectors so as to satisfy the continuity (for the velocity vectors) and equilibrium (for the force vectors) principles at each junction:

$$\mathbf{v}_t = \mathbf{v}_{sr}, \quad \mathbf{f}_t = -\mathbf{f}_{sr} \tag{16}$$

If Eqs.(16) are substituted into Eq.(12) the source-radiating force vector and force radiating velocity vector can be related through the following impedance expression:

$$\mathbf{f}_{sr} = -\mathbf{Z}_t \mathbf{v}_{sr} \tag{17}$$

Substitution of Eq.(17) into Eq. (13) yields:

$$\mathbf{v}_{sr} = -\mathbf{Y}_{sr,sr}\mathbf{Z}_t\mathbf{v}_{sr} + \mathbf{Y}_{sr,pf}\mathbf{f}_{pf} + \mathbf{Y}_{sr,c}\mathbf{f}_c, \quad \mathbf{v}_{sr} = \left(\mathbf{I} + \mathbf{Y}_{sr,sr}\mathbf{Z}_t\right)^{-1}\left(\mathbf{Y}_{sr,pf}\mathbf{f}_{pf} + \mathbf{Y}_{sr,c}\mathbf{f}_c\right) \tag{18}$$

$$\mathbf{v}_{sr} = \left(\mathbf{I} + \mathbf{Y}_{sr,sr}\mathbf{Z}_t\right)^{-1}\mathbf{Y}_{sr,pf}\mathbf{f}_{pf} + \left(\mathbf{I} + \mathbf{Y}_{sr,sr}\mathbf{Z}_t\right)^{-1}\mathbf{Y}_{sr,c}\mathbf{f}_c, \quad \mathbf{v}_{sr} = \mathbf{Q}_{tp}\mathbf{f}_{pf} + \mathbf{Q}_{tc}\mathbf{f}_c \tag{19}$$

where the matrices $\mathbf{Q}_{tp}$ and $\mathbf{Q}_{tc}$ are given by:

$$\mathbf{Q}_{tp} = \left(\mathbf{I} + \mathbf{Y}_{sr,sr}\mathbf{Z}_t\right)^{-1}\mathbf{Y}_{sr,pf}, \quad \mathbf{Q}_{tc} = \left(\mathbf{I} + \mathbf{Y}_{sr,sr}\mathbf{Z}_t\right)^{-1}\mathbf{Y}_{sr,c} \tag{20}$$

Using now Eq.(17) with Eq.(19) gives the source-radiating force vectors:

$$\mathbf{f}_{sr} = -\mathbf{Z}_t\mathbf{Q}_{tp}\mathbf{f}_{pf} - \mathbf{Z}_t\mathbf{Q}_{tc}\mathbf{f}_c, \quad \mathbf{f}_{sr} = \mathbf{R}_{tp}\mathbf{f}_{pf} + \mathbf{R}_{tc}\mathbf{f}_c \tag{21}$$

where $\mathbf{R}_{tp}$ and $\mathbf{R}_{tc}$ are given by:

$$\mathbf{R}_{tp} = -\mathbf{Z}_t\mathbf{Q}_{tp}, \quad \mathbf{R}_{tc} = -\mathbf{Z}_t\mathbf{Q}_{tc} \tag{22}$$

Similar to Eq.(13), the control velocity vector can also be expressed using the mobility method:

$$\mathbf{v}_c = \mathbf{Y}_{c,sr}\mathbf{f}_{sr} + \mathbf{Y}_{c,pf}\mathbf{f}_{pf} + \mathbf{Y}_{c,c}\mathbf{f}_c \tag{23}$$

where the mobility matrices have the form:

$$\mathbf{Y}_{c,sr} = \begin{bmatrix} \mathbf{Y}_{c,s} & \mathbf{0} \\ \mathbf{0} & \mathbf{Y}_{c,r} \end{bmatrix}, \quad \mathbf{Y}_{c,pf} = \begin{bmatrix} \mathbf{Y}_{c,pfs} & \mathbf{0} \\ \mathbf{0} & \mathbf{Y}_{c,pfr} \end{bmatrix}, \quad \mathbf{Y}_{c,c} = \begin{bmatrix} \mathbf{Y}_{c,cs} & \mathbf{0} \\ \mathbf{0} & \mathbf{Y}_{c,cr} \end{bmatrix} \tag{24}$$

$\mathbf{Y}_{c,s}$, $\mathbf{Y}_{c,pfs}$, $\mathbf{Y}_{c,cs}$ and $\mathbf{Y}_{c,r}$, $\mathbf{Y}_{c,pfr}$, $\mathbf{Y}_{c,cr}$ are mobility matrices of the source and the radiating panel, at the control locations. Substitution of the right term of Eq.(21) into Eq.(23) yields:

$$\mathbf{v}_c = \mathbf{Y}_{c,sr}\mathbf{R}_{tp}\mathbf{f}_{pf} + \mathbf{Y}_{c,sr}\mathbf{R}_{tc}\mathbf{f}_c + \mathbf{Y}_{c,pf}\mathbf{f}_{pf} + \mathbf{Y}_{c,c}\mathbf{f}_c, \qquad \mathbf{v}_c = \left(\mathbf{Y}_{c,sr}\mathbf{R}_{tp} + \mathbf{Y}_{c,pf}\right)\mathbf{f}_{pf} + \left(\mathbf{Y}_{c,sr}\mathbf{R}_{tc} + \mathbf{Y}_{c,c}\right)\mathbf{f}_c \tag{25}$$

$$\mathbf{v}_c = \mathbf{T}_{cp}\mathbf{f}_{pf} + \mathbf{T}_{cc}\mathbf{f}_c \tag{26}$$

where $\mathbf{T}_{cp}$ and $\mathbf{T}_{cc}$ are given by:

$$\mathbf{T}_{cp} = \mathbf{Y}_{c,sr}\mathbf{R}_{tp} + \mathbf{Y}_{c,fp}, \qquad \mathbf{T}_{cc} = \mathbf{Y}_{c,sr}\mathbf{R}_{tc} + \mathbf{Y}_{c,c} \tag{27}$$

With feedback control, the control force vector $\mathbf{f}_c$ is related to the control velocity vector $\mathbf{v}_c$ by means of the control law matrix $\mathbf{H}$:

$$\mathbf{f}_c = -\mathbf{H}\mathbf{v}_c \tag{28}$$

so that the control velocities can be calculated using Eq.(26) as follows:

$$\mathbf{v}_c = \mathbf{T}_{cp}\mathbf{f}_{pf} + \mathbf{T}_{cc}\left(-\mathbf{H}\mathbf{v}_c\right), \qquad \mathbf{v}_c = \left(\mathbf{I} + \mathbf{T}_{cc}\mathbf{H}\right)^{-1}\mathbf{T}_{cp}\mathbf{f}_{pf} \tag{29}$$

whereas the source and radiating panel forces are determined by the right term of Eq.(21). Details on how the control matrix $\mathbf{H}$ is populated can be found in (7). Finally, the source and radiating velocities are then given by Eq.(13). The sound power radiated by the radiating panel can then be evaluated using the velocities of the radiating elements which are a subset of $\mathbf{v}_{sr}$, the right term of Eq.(4), as:

$$W(\omega) = \mathbf{v}_{re}^H \mathbf{R}\mathbf{v}_{re} \tag{30}$$

where $\mathbf{R}$ is the radiation resistance matrix and $(\,)^H$ denotes the Hermitian transpose (the complex conjugate). The sound power of the incident plane wave can be calculated using the following expression

$$W_i = \left|P^2\right| \frac{l_x l_y}{2\rho c} \cos\theta \tag{31}$$

where ρ and c are the air density and the speed of sound. The sound power transmission ratio can be calculated as $T = W/W_i$.

3. EXPERIMENTAL SETUP

The experimental study is carried out on a prototype double panel which is shown in Figure 2.

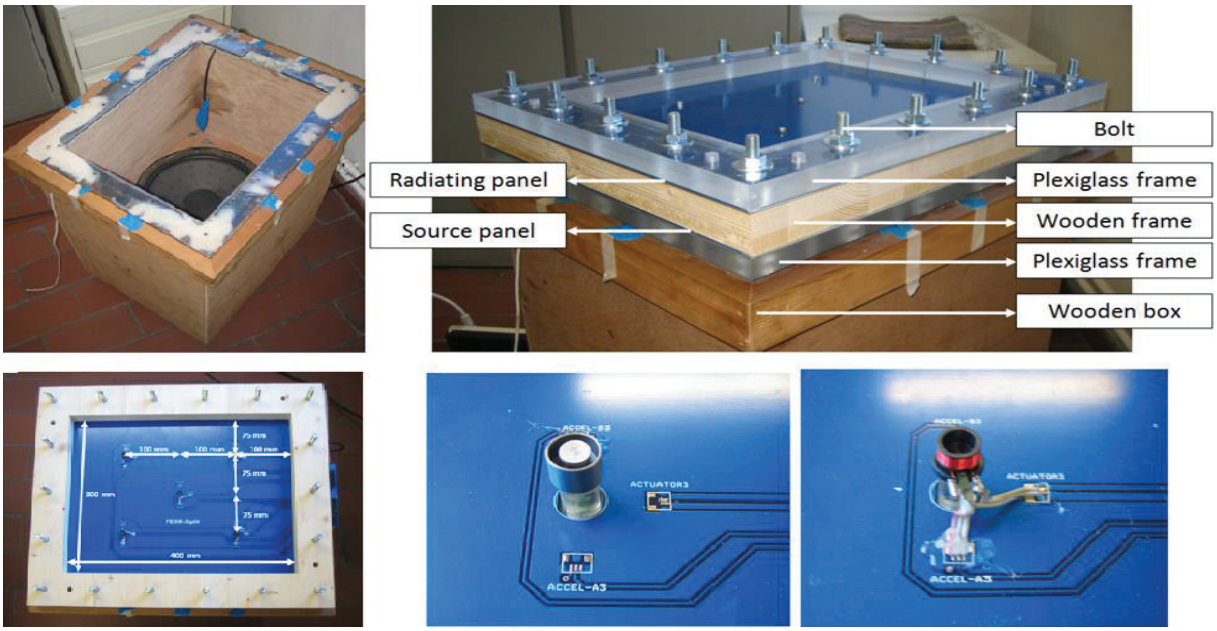

Figure 2 – Experimental setup

The unconstrained *x,y* - dimensions of the panels are 0.3×0.4 m. They are made of a fiberglass reinforced epoxy used for PCB boards. The width of the air cavity between them is 0.036 m. The prototype panel is mounted on top of the open side of wooden box with thick and heavy walls with the inner dimensions of 0.3×0.4×0.5 m. The box has a loudspeaker with a 30 cm membrane diameter to produce high levels of sound pressure inside the box at low frequencies. The thick and heavy box side walls ensure that the flanking sound power radiated through the walls is at least 20 dB lower than that radiated through the panel. White noise signal is used to drive the loudspeaker. A reference microphone is located in a corner inside the box, whereas the measurement microphone is located outside, 10 centimetres above the radiating panel centre. The sound transmission ratio is approximated by the FRF between the sound pressure measured by the outside microphone and the reference microphone inside. The double panel system is equipped with a miniature voice coil actuator, (8), mounted at its centre, in the air cavity between the two panels. Its mechanical terminals are attached to the two panels so that it can react against them. One miniature MEMS accelerometer, (9), is attached at the actuator footprint at the radiating panel. Its time-integrated output, proportional to the radiating panel velocity at the actuator junction point, is amplified and fed back to the actuator as the error signal. The time integration is performed with an analogue integrator with a 1 Hz cut-off frequency. In such a way a skyhook damper is realised (10,11). In order to ensure the stability of the feedback loop, it is necessary that the uncoupled source panel fundamental natural frequency is higher than that of the uncoupled radiating panel. Analytical stability analyses carried out previously with simple lumped parameter 2 DOF models providing more details on why this is necessary to ensure stability can be found in references (12–14). In this study the prototype panels were fabricated with slightly different thicknesses: 2 mm for the source panel and 1.5 mm for the radiating panel so as to ensure that the fundamental natural frequency of the source panel is higher than that of the radiating panel.

4. RESULTS AND DISCUSSION

The stability analysis is carried out using the Nyquist criterion by studying the properties of the open-loop sensor-actuator frequency response function (FRF). The corresponding Bode and Nyquist plots determined theoretically and experimentally are shown in Figure 3.

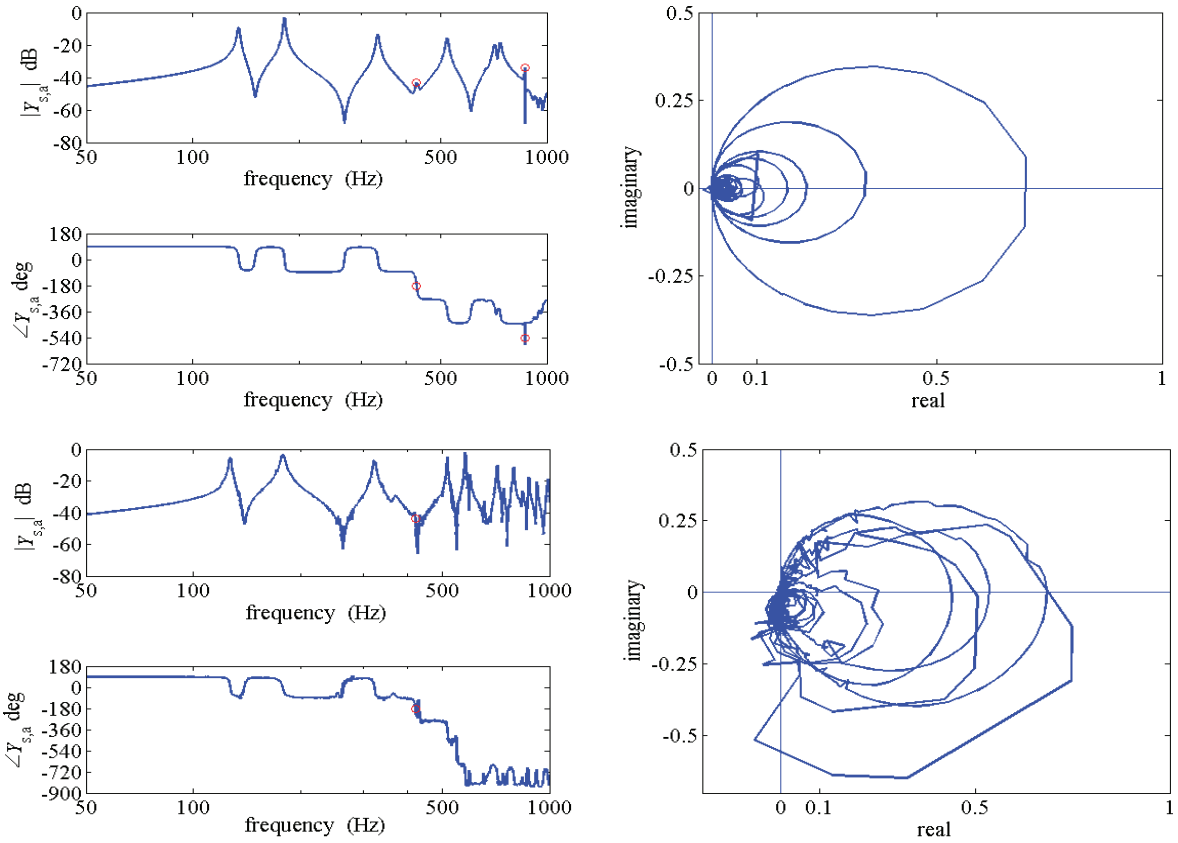

Figure 3 – Bode and Nyquist plots of the open loop sensor-actuator FRF. Up: simulated, bottom: measured

The simulated and measured results agree reasonably well. The FRF behaves as if the sensor-actuator pair were collocated up to approximately 400 Hz. Above this frequency phase lags occur due to higher order modes so that the feedback loop is conditionally stable. The frequencies at which the Nyquist locus crosses the negative real axis are shown in Bode plots using the red circles. The amplitudes of the FRF at the crossover frequencies are much smaller that the FRF amplitudes at the structural resonances. Therefore, a relatively large gain margin enables implementing large feedback gains and generating large active damping effects. This is illustrated in Figure 4, which shows the sound power transmission ratio with and without control, both simulated and measured. The two plots suggest that large sound transmission occurs due to the two fundamental resonances of the double panel system occurring at 135 Hz and 181 Hz.

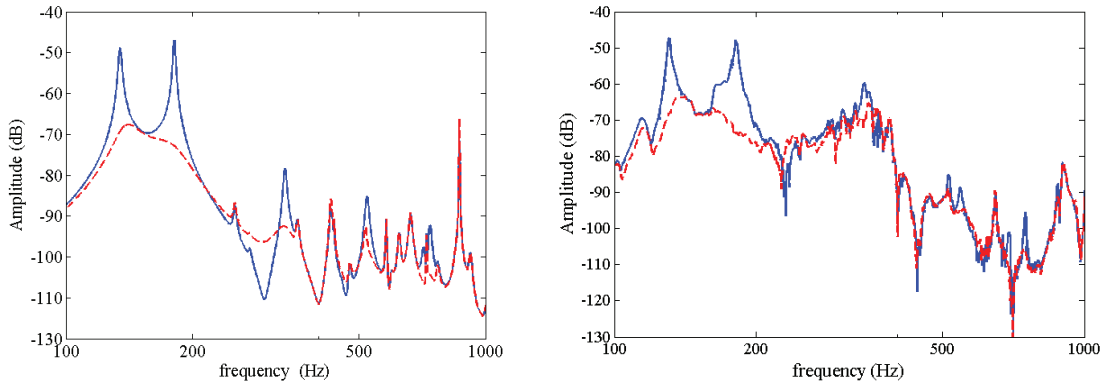

Figure 4– The sound power transmission ratio. Left: simulated, right: measured. Solid, blue lines: no control, dashed red lines: with control.

This is because the two corresponding structural modes are characterized by large volumetric components of the radiating panel vibration, as shown in Figure 5. Above the second resonance (the mass-air-mass mode shown in Figure 5) the sound transmission ratio rolls off steeply with frequency since the vibration of the two panels and the sound transmission become governed by the mass law, Figure 4. Therefore the active reduction of the sound transmission at frequencies below the mass-air-mass resonance is important. As shown by the red dashed lines, reductions of about 20 dB are both anticipated theoretically (Figure 4, left plot) and determined experimentally (Figure 4, right plot). The simulation and experimental results agree well, except that the (0,0,1) acoustical mode of the wooden box air cavity causes a resonance at about 340 Hz in the experimentally determined sound power transmission ratio. Note that the theoretical model does not include the acoustics of the rectangular air cavity beneath the source panel.

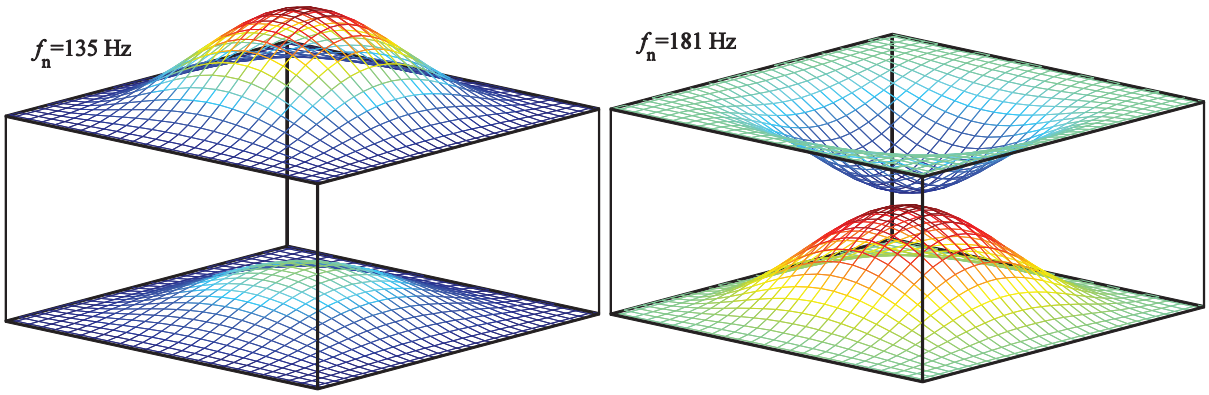

Figure 5– The two fundamental modes of the double panel. Left: first mode, right: mass-air-mass mode

CONCLUSIONS

The active control of sound transmission through a double panel using a skyhook damper located in the air cavity between the source and the radiating panel is investigated theoretically and experimentally. The stability analysis indicates that the feedback loop is surprisingly robust with respect to the non-collocated sensor-actuator arrangement. The arrangement is non-collocated because the reactive force actuator is collocated (and dual) to the sensor measuring relative velocity across its terminals. However in the present scheme an absolute velocity sensor at the radiating panel actuator terminal is used to provide the error signal. Although the theoretical foundation for this type of active vibration control have been laid for lumped parameter systems in the past, in this study it is shown both experimentally and theoretically that this kind of control scheme can be successfully used in distributed parameter systems. In particular, it is shown that the sound power transmission ratio through double panels can be significantly reduced in the low frequency range, below the mass-air-mass resonance. This is important because at those frequencies the acoustic and structural wavelengths are large so that the effectiveness of traditional passive treatments such as sound absorbing foams or viscoelastic constrained damping layers is unsatisfactory. Therefore active control can be used as a viable alternative to passive sound transmission control methods in order to reduce the very low frequency sound transmission.

ACKNOWLEDGEMENTS

This project has received funding from the European Union's Horizon 2020 research and innovation programme under the Marie Sklodowska-Curie grant agreement no. 657539.

REFERENCES

1. Mixson JS, Barton CK, Vaicaitis R. Interior Noise Analysis and Control for Light Aircraft. 1977. Available from: doi:10.4271/770445
2. Fahy F (Frank J., Gardonio P. *Sound and structural vibration : radiation, transmission and response*. Elsevier/Academic; 2007. 633 p.
3. Elliott SJ, Johnson ME. Radiation modes and the active control of sound power. *The Journal of the Acoustical Society of America*. [Online] 1993;94(4): 2194–2204. Available from: doi:10.1121/1.407490
4. Fahy F, Walker J. *Advanced applications in acoustics, noise, and vibration*. Spon Press; 2004. 640 p.
5. Cox TJ, D'Antonio P. *Acoustic absorbers and diffusers : theory, design and application*. Taylor & Francis; 2009. 476 p.
6. Alujević N, Gardonio P, Frampton KD. Smart double panel with decentralized active dampers for sound transmission control. *AIAA Journal*. [Online] 2008;46(6). Available from: doi:10.2514/1.32369
7. Alujeví N, Gardonio P, Frampton KD. Smart double panel for the sound radiation control: Blended velocity feedback. *AIAA Journal*. [Online] 2011;49(6): 1123–1134. Available from: doi:10.2514/1.44284
8. *Non-Comm DC Voice Coil Linear Actuator - NCC01-04-001-1X*. [Online] Available from: https://www.h2wtech.com/product/voice-coil-actuators/NCC01-04-001-1X
9. *Precision ±1.7 g, ±5 g, ±18 g Single-/Dual-Axis iMEMS® Accelerometer*. [Online] Available from: http://www.alldatasheet.com/datasheet-pdf/pdf/527888/AD/ADXL103CE.html
10. Karnopp DC, Trikha AK. Comparative Study of Optimization Techniques for Shock and Vibration Isolation. *Journal of Engineering for Industry*. [Online] American Society of Mechanical Engineers; 1969;91(4): 1128–1132. Available from: doi:10.1115/1.3591760
11. Kaplow CE, Velman JR. Active Local Vibration Isolation Applied to a Flexible Space Telescope. *Journal of Guidance, Control, and Dynamics*. [Online] 1980;3(3): 227–233. Available from: doi:10.2514/3.55976
12. Alujević N, Čakmak D, Wolf H, Jokić M. Passive and active vibration isolation systems using inerter. *Journal of Sound and Vibration*. [Online] 2018;418: 163–183. Available from: doi:10.1016/j.jsv.2017.12.031
13. Caiazzo A, Alujević N, Pluymers B, Desmet W. Active control of turbulent boundary layer-induced sound transmission through the cavity-backed double panels. *Journal of Sound and Vibration*. [Online] 2018;422: 161–188. Available from: doi:10.1016/j.jsv.2018.02.027
14. Alujević N, Wolf H, Gardonio P, Tomac I. Stability and performance limits for active vibration isolation using blended velocity feedback. *Journal of Sound and Vibration*. [Online] 2011;330(21): 4981–4997. Available from: doi:10.1016/j.jsv.2011.05.020